Van der Waals epitaxial MOCVD-growth of $(Bi_xSb_{1-x})_2Te_3$ (0<x<1) films

G. Bendt,[1] J. Sonntag,[2] A. Lorke,[2] W. Assenmacher,[3] U. Hagemann,[4] S. Schulz[1]*

[1] Institute of Inorganic Chemistry and Center for Nanointegration Duisburg-Essen (CENIDE), University of Duisburg-Essen, Universitätsstr. 5-7, D-45117 Essen, Germany. Fax: 44 0201 1833830; Tel: 44 0201 1834635; E-mail: stephan.schulz@uni-due.de

[2] Faculty of Physics and Center for Nanointegration Duisburg-Essen (CENIDE), University of Duisburg-Essen, Lotharstraße 1, D-47048 Duisburg, Germany

[3] Institute of Inorganic Chemistry, University of Bonn, Römerstr. 164, D-53117 Bonn, Germany.

[4] Interdisciplinary Center for Analytics on the Nanoscale (ICAN), NETZ, Carl-Benz-Str. 199, D-47047 Duisburg, Germany

Abstract

Epitaxial $(Bi_xSb_{1-x})_2Te_3$ with (0<x<1) were grown by MOCVD process at 400 °C using the tailor-made precursors Et_2Te_2, i-Pr_3Sb and Et_3Bi. The films grown on Al_2O_3(0001) substrates show a very smooth surface morphology as was shown by SEM, AFM and TEM, while those grown on Si(100) are rather polycrystalline. The chemical composition of the crystalline films (XRD) was investigated by EDX and XPS and the in-plane transport properties were measured and a strong dependency from the bismuth content was found, which allows the tuning of the carrier concentration and mobility in a wide range.

Introduction

Thermoelectric materials have attracted considerable attention in recent years since the thermoelectric effect allows the direct conversion of thermal energy into electrical energy and *vice versa*.[1-5]. Systematic research in this field began in the 1950´s and resulted in the development of radioisotope thermoelectric generators (RTG), which provide for example the energy supply of satellites and space probes.[6] The energy conversion efficiency of thermoelectric materials is given by a dimensionless figure of merit $ZT = \alpha^2\sigma T/(\kappa_e + \kappa_L)$, where α is the Seebeck coefficient, σ the electrical conductivity, T the absolute temperature and κ_e and κ_L the thermal conductivities of the electron component and the lattice component, respectively. Consequently, a good thermoelectric material must exhibit a high Seebeck coefficient and electrical conductivity, whereas its thermal conductivity should be as low as possible.

Presently, the best thermoelectric materials for near-room temperature applications are binary group VI-tellurides, Sb_2Te_3 and Bi_2Te_3, and their ternary solid solution $(Bi_xSb_{1-x})_2Te_3$ (0<x<1), respectively, which are narrow bandgap semiconductors with layered tetradymite-type structures.[7,8] The structure is built by a close packing of tellurium atoms perpendicular to the *c*-axis in *R*-3*m*:H with the stacking sequence *chh* in Jagodzinski-symbols, occupying octahedral sites except in every third layer of Te_6 Octahedra. The stacking sequence is (*AγB□AγBαC□BαCβA□Cβ*) and thus, double layers of edge-sharing $Bi(Sb)Te_6$ octahedra consisting of 5 atom layers (quintuple layers) with the sequence Te1-Bi(Sb)-Te2-Bi(Sb)-Te1 are formed. Each double layer of octahedra (quintuple layer) has the composition $(Bi(Sb))_2Te_3$, which is a condition for layer structures. Three formula units are within the unit cell and so 3 stacks of the quintuple layers, which are connected via weak van der Waals bonding, whereas the bonding inside the layer is dominated by mixed covalent-ionic type.

The interest in Bi_2Te_3 thin films and related materials such as Bi_2Se_3 and Sb_2Te_3 recently received a second major boost since they are archetypes of materials referred to as *topological insulators*,[9-11] which are characterized by the topologically protected conducting surface-states forming a single spin-polarized Dirac cone on the bulk insulating interior due to strong spin–orbit coupling.[12-16] Very recently, it was demonstrated that the topological surface states can be modulated and insulating bulk states can be achieved in solid-solution $(Bi_xSb_{1-x})_2Te_3$.[17]

ZT values of thermoelectric materials can be enhanced by nanostructuring approaches,[18-21] since the thermal conductivity in low-dimensional nanostructures is decreased due to efficient phonon scattering at boundaries and interfaces, while the Seebeck coefficient is simultaneously increased because of quantum confinement effects and the modification of the electronic band structure.[22,23] In addition, the synthesis of solid solutions in the quasi binary system Bi_2Te_3-Sb_2Te_3 has been established for ZT value improvement. $(Bi_xSb_{1-x})_2Te_3$ compounds for instance show enhanced ZT values compared to the corresponding binary materials (Bi_2Te_3, Sb_2Te_3) due to additional phonon scattering introduced by lattice disordering (site disordering), which strongly reduces the thermal conductivity. Moreover, the formation of *antisite* defects, i.e. the occupation of tellurium sites by pnictogen atoms, is suppressed with increasing bismuth content due to the enhanced electronegativity difference, which leads to a higher defect formation energy, a decreased carrier concentration and an increased Seebeck coefficient. Transport properties of $(Bi_xSb_{1-x})_2Te_3$ single crystals were investigated using theoretical and experimental methods and a maximum room temperature figure of merit $Z = 3.2 \times 10^{-3}$ K^{-1} was determined for the solid solution,[24,25] while *p*-type $(Bi_xSb_{1-x})_2Te_3$ nanocomposites showed the maximum room temperature Z of 3.52×10^{-3}/K for $(Bi_{0.2}Sb_{0.8})_2Te_3$.[26] Poudel et al. reported on record-high ZT values of 1.4 at 373 K for bulk $(Bi_xSb_{1-x})_2Te_3$ with embedded nanostructures[1] while Xie et al. reported on high performance p-type $Bi_{0.52}Sb_{1.48}Te_3$ material with a maximum ZT value of 1.56 at 300 K, which is roughly a 50% improvement compared to commercial Bi_2Te_3 materials.[27]

While the synthesis of bulk as well as nanostructured p-type $(Bi_xSb_{1-x})_2Te_3$ is well established,[1,28-33] reports on the growth of high quality epitaxial thin films of these materials are rather scare.[34] Ternary $(Bi_xSb_{1-x})_2Te_3$ thin films with a very limited range of x values were fabricated by molecular beam epitaxy,[35] physical vapor deposition,[36] mechanical alloying, [37,38], dc magnetron sputtering[39] and potentiostatic electrodeposition.[40] $Bi_{0.5}Sb_{1.5}Te_3$ is the best commercially available p-type thermoelectric material at room temperature and many efforts have been made to improve the performance of $(Bi_xSb_{1-x})_2Te_3$ films.[41] However, the growth of such ternary films with specific preferential crystal growth on the substrate is still challenging. In addition, these films often show low power factors, since the carrier concentrations in many films often range from $10^{20}/cm^3$–$10^{21}/cm^3$, which exceed the optimal value of carrier concentration of

roughly 10^{19}/cm^3[41] and limit the Seebeck coefficient. Moreover, ternary $(Bi_xSb_{1-x})_2Te_3$ material films with a broad variation of x were only scarcely realized in electrochemically synthesized $(Bi_xSb_{1-x})_2Te_3$ thin films[42] and by magneton co-sputtering.[43]

The MOCVD process, which has been established in the past for the deposition of high quality films of the binary materials including Bi_2Te_3/Sb_2Te_3 superlattices by the so-called Van der Waals epitaxy[44-46] was much less used for ternary film deposition.[47,48] $(Bi_xSb_{1-x})_2Te_3$ films were successfully grown using *i*-Pr_2Te, Me_3Bi and Et_3Sb as metal organic precursors.[49,50] Very recently, high quality $(Bi_{0.53}Sb_{0.47})_2Te_3$ thin films with atomically sharp interfaces and without any interfacial layers were grown by van der Waals epitaxy on a GaSe buffer layer.[51] We have recently demonstrated the MOCVD growth of epitaxial Sb_2Te_3 films and investigated their valence band structure by angle-resolved photoemission spectroscopy.[52] Here, we report on the deposition of $(Bi_xSb_{1-x})_2Te_3$ thin films over the entire range from Bi_2Te_3 to Sb_2Te_3 (x = 0 - 1) at temperatures below 400 °C using *i*-Pr_3Sb, Et_3Bi and Et_2Te_2 as alternate metal organic precursors for low-temperature MOCVD film deposition. Low growth temperatures are advantageous in order to suppress interdiffusion in these films, which becomes problematic when using the standard Bi precursor Me_3Bi due to its rather high thermal stability. The composition and morphology of the resulting epitaxial thin films was studied in detail and their electric conductivity was determined.

Experimental Details

MOCVD Deposition. MOCVD studies were performed in a cold-wall high-vacuum MOCVD reactor. $(Bi_xSb_{1-x})_2Te_3$ films were deposited on either Si(100) or Al_2O_3(0001) substrates within 15 minutes at a working pressure of 10 mbar. Si(100) substrates were degreased with acetone, treated with hydrofluoric acid and heated to 500 °C at 10^{-3} mbar for 1 hour in the reactor. Al_2O_3(0001) substrates were degreased with acetone and cleaned with a 3:1 mixture of sulfuric acid and phosphoric acid. Et_2Te_2,[53] *i*-Pr_3Sb[54] and Et_3Bi,[55] which were synthesized by (slightly modified) literature methods, were loaded into glass bubblers attached to the MOCVD-reactor under inert conditions (Ar). Argon was used as carrier gas, and the flow rate of the precursors (40 sccm Et_2Te_2, 5 sccm *i*-Pr_3Sb and 5 sccm Et_3Bi) was controlled by use of a mass flow controller (MKS Instruments). The flow of the precursors was adjusted by the bubbler temperature (*i*-Pr_3Sb: -25 °C to -5 °C; Et_3Bi: -50 °C to -30 °C;

Et_2Te_2: +20 °C). After the film deposition was finished, the system was cooled to ambient temperature within 30 minutes under vacuum.

DSC Analysis. A DSC 200 Phox (Netzsch Gerätebau) was used for differential scanning calorimetry (DSC) analyses.

X-ray Analysis. XRD patterns were obtained using a Bruker D8 Advance powder diffractometer with Cu K_α radiation (λ: 1.5418 Å).

X-ray photoelectron spectroscopy. XPS studies were performed using a Versaprobe II™ (Ulvac-Phi) with monochromatic Al Kα light at 1486.6 eV photon energy. For depth-profiling this machine is equipped with an Ar-sputter source. The emission angle between analyzer and sample is 45°.

Surface-Analysis. The surface morphology of the Sb_2Te_3-film was investigated by AFM using an AFM Veeco diInnova and by SEM using a Jeol JSM 6510 equipped with an energy dispersive X-ray spectroscopy (EDX) device (Bruker Quantax 400). A cross section sample of the Sb_2Te_3 film was prepared by use of a Jeol Cross-Section Polisher (IB-09010CP).

Transmission electron microscopy. TEM studies were conducted on a transmission electron microscope FEI Philips CM30 T/LaB6 operated at 300 kV, equipped with a Gatan CCD for image recording and with a Thermo NSS systems for EDX analysis using a Si(Li) Nanotrace detector. Cross section samples of the coated substrates prepared by focused ion beam (FIB) thinning were prepared using a FEI Helios NanoLab™ 600.

Results and Discussion

The standard tellurium precursor for MOCVD applications is dimethyltellane Me_2Te. Me_2Te is liquid at room temperature (b.p. 82 °C) and has a sufficiently high vapor pressure (40.6 Torr, 20 °C),[56] but is thermally very stable and requires high thermolysis temperatures of 500 °C in H_2 atmosphere to be fully decomposed.[57] In addition, the decomposition occurs under formation of methyl radicals, a potential source for carbon contamination. The decomposition temperatures of dialkyltellanes containing longer C-chains with additional branching (Et_2Te, *i*-Pr_2Te, *t*-Bu_2Te) typically decreases due to an increased stability of the resulting radicals.[57,58] Moreover, β-hydride elimination reactions on the surface of the substrate have to be taken into account.[59-61] In order to achieve the lowest possible substrate temperature to prevent the loss of tellurium out of the film, we used

diethylditellane Et_2Te_2 as Te source and reported on its thermal properties in our previous report [52]. Et_2Te_2 was suggested to decompose in a two-step mechanism as was also reported by Kisker et al. for Me_2Te_2.[62] First, Et_2Te_2 disproportiones into elemental tellurium and diethyl tellane, which then thermally degrades at higher temperature, leading to a high tellurium concentration at the growth front. *i*-Pr_3Sb and Et_3Bi were used as Sb and Bi precursor due to their comparable decomposition temperatures of roughly 250 °C and 230 °C, respectively.

$(Bi_xSb_{1-x})_2Te_3$ films were deposited at 400 °C on $Al_2O_3(0001)$ substrates. They are typically highly reflective and the SEM images show the formation of dense, flat films over the entire range of the Al_2O_3substrate (Fig 1a). In contrast, the films deposited on Si(100) at 400 °C are dull and grey and extremely rough according to REM studies. They consist of hexagonal platelets lying either flat to the substrate or standing perpendicular on the surface (Fig. 1b).

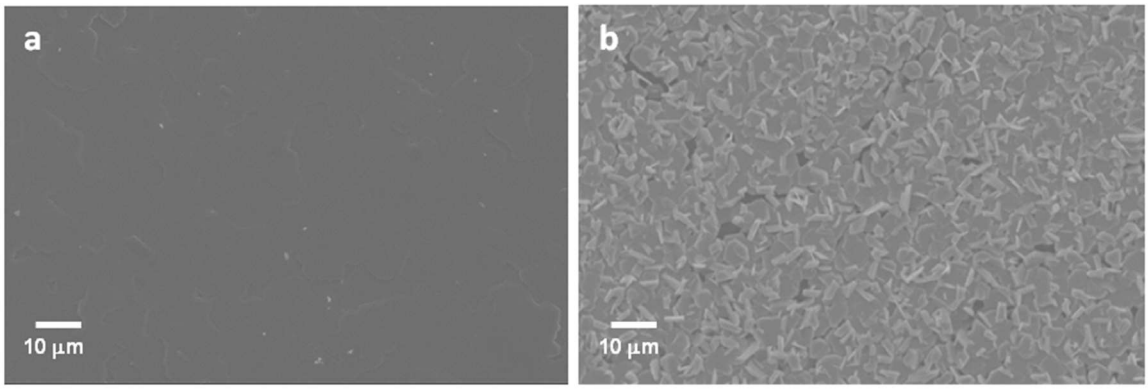

Fig. 1. SEM images of $(Bi_{0.5}Sb_{0.5})_2Te_3$ films grown on $Al_2O_3(0001)$ (a) and Si(100) (b) at 400 °C.

Binary antimony and bismuth telluride M_2Te_3 (M = Sb, Bi) as well as its ternary tellurides are described in the space group *R*-3*m*:H *(No. 166)* and form layered, rhombohedral crystal structures built by anisotropic layers, in which five atomic planes are covalently bonded to form a Te(1)-M-Te(2)-M-Te(1) quintuple layer. The conventional unit cell includes three quintuple layers, which are interconnected by weak van der Waals force. An AFM micrograph of a $(Bi_{0.5}Sb_{0.5})_2Te_3$ film grown on $Al_2O_3(0001)$ shows regular terraces of 1 nm height (Fig. 2), which corresponds to one quintuple layer of the layered tetradymite-type structure of M_2Te_3, that is roughly 1 nm thick. These findings confirm a layered growth as was previously observed in MBE-grown M_2Te_3 films.[63]

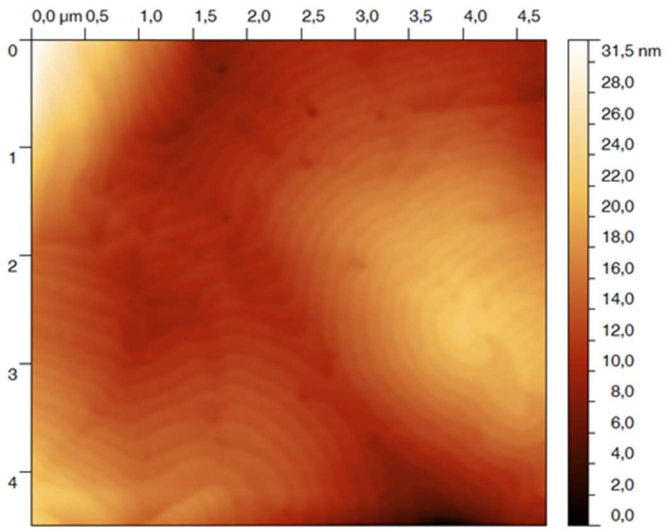

Fig. 2. AFM photographs of a $(Bi_{0.5}Sb_{0.5})_2Te_3$ film grown on $Al_2O_3(0001)$ at 400 °C.

The chemical composition of the films was measured by EDX analysis. The measurements clearly showed that the composition for each film is close to the ideal 40:60 (Sb/Bi:Te) molar ratio. The XRD pattern, measured in Θ-2Θ (Bragg-Brentano) set-up for the MOCVD grown films on $Al_2O_3(0001)$ is displayed in fig. 3.

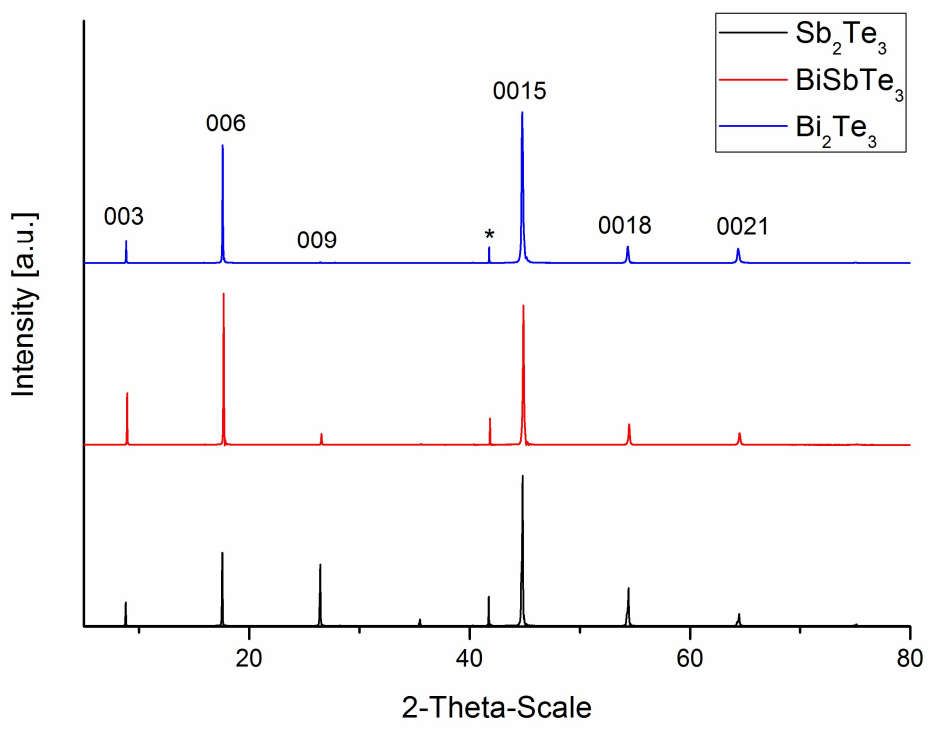

Fig. 3. X-ray diffractograms of Sb_2Te_3 (black), Bi_2Te_3 (blue) and $(Bi_{0.5}Sb_{0.5})_2Te_3$ films (red) grown on $Al_2O_3(0001)$ at 400 °C.

All observed Bragg-peaks can be indexed on the basis of rhombohedral Sb_2Te_3 (JCPDS card 15-0874) or Bi_2Te_3 (JCPDS card 15-0863), respectively. The small FWHM of the peaks indicate a high degree of crystallinity. Only diffraction peaks related to the 00*l* crystal planes are visible, whereas other peaks compared to the standard card are totally suppressed, indicating the growth direction to be perfectly aligned along the (00*l*) crystal orientation with the *c*-axis of the tetradymite lattice perpendicular to the substrate surface. No peaks for other phases or impurities such as Bi_2O_3, Sb_2O_3 TeO_2 or elemental Te were detected.

In contrast, the XRD pattern for $(Bi_xSb_{1-x})_2Te_3$ films grown on Si(100) substrates unexceptionally show strong texture effects as is shown in Fig. 4 for a $(Bi_{0.5}Sb_{0.5})_2Te_3$ film. The diffractogram shows enhanced peak intensities for the 00*l* reflexes, but other peaks are clearly visible and confirm the two preferred orientations of the platelets in the film as observed by SEM.

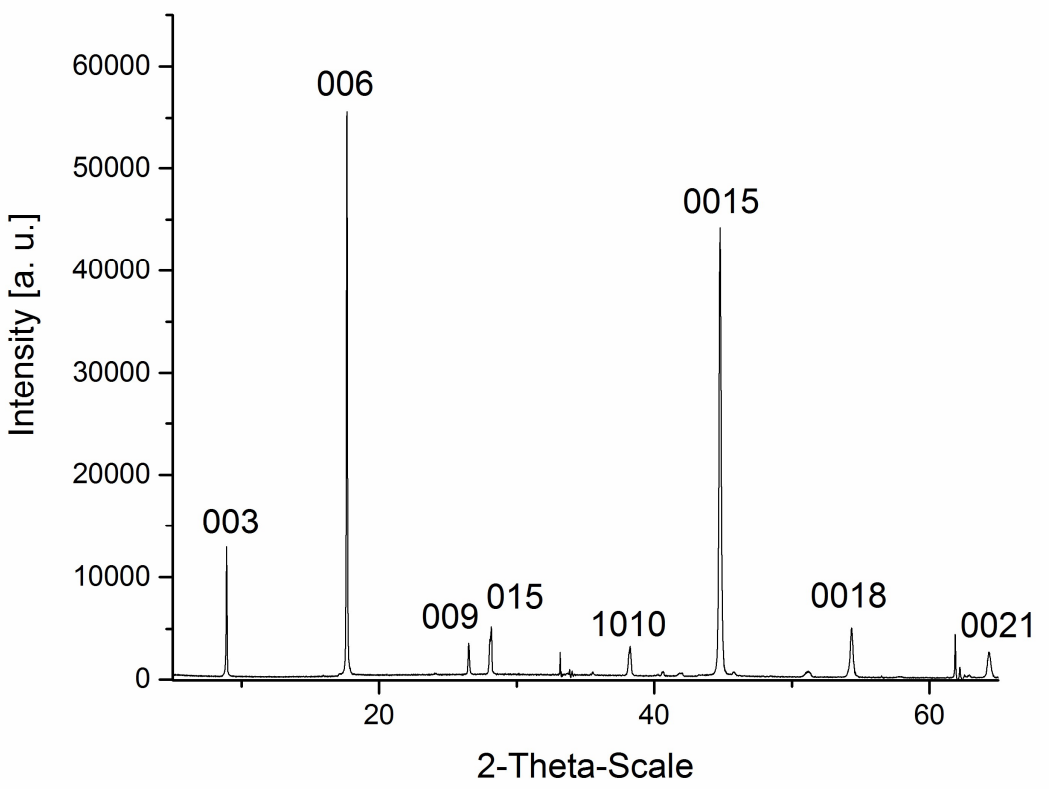

Fig. 4. X-ray diffractogram of a $(Bi_{0.5}Sb_{0.5})_2Te_3$ film grown on Si(100) at 400 °C.

Figure 5 shows the 006 pole figures of $(Bi_{0.5}Sb_{0.5})_2Te_3$ films grown on Al_2O_3(0001) (left) and Si(100) (right) at 400 °C. The epitaxial $(Bi_{0.5}Sb_{0.5})_2Te_3$ film grown on Al_2O_3 only shows a single peak, while the 0006 pole figure of the film grown on Si shows a pattern due to the

hexagonal discs standing on the substrate surface. The epitaxial relationship of the film and the Al_2O_3 substrate is $(Bi_{0.5}Sb_{0.5})_2Te_3$ (001)‖Al_2O_3(0001).

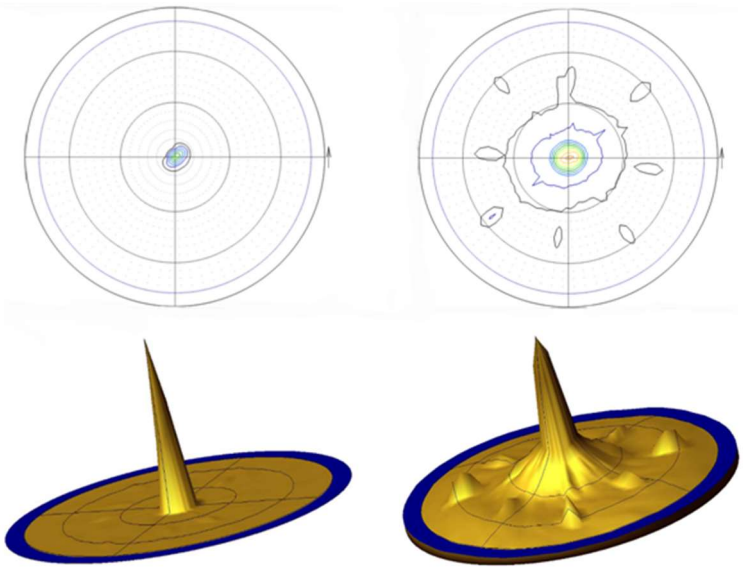

Fig. 5. 006 pole figures for $(Bi_{0.5}Sb_{0.5})_2Te_3$ films grown on Al_2O_3(0001) (left) and Si(100) (right).

X-Ray photoelectron spectroscopy (XPS) is a surface sensitive method for the determination of the chemical environment of an element. An XPS measurement for a $(Bi_{0.5}Sb_{0.5})_2Te_3$ film grown at 400 °C on Al_2O_3(0001) shows the expected peaks for Bi 4f7/2and Bi 4f5/2 at 157.5 and 162.8 eV, Sb 3d3/2 and 3d5/2 at 538.3 and 528.8 eV, Te 3d3/2 and 3d5/2 at 582.9 and 572.5 eV (Sb spectra shown in Fig. 6).

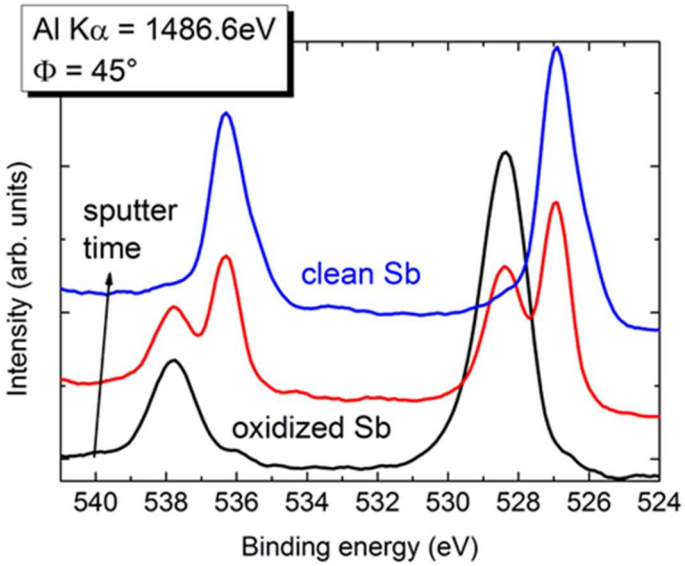

Fig. 6. X-Ray photoelectron spectrum of the $(Bi_{0.5}Sb_{0.5})_2Te_3$ film grown on Al_2O_3(0001) with native oxidized surface (black) and after 1.5 min (5 nm, red) and 3 min sputtering time (= 10 nm, blue).

These values are in good agreement with reported binding energies in Sb_2Te_3 and Bi_2Te_3, respectively. In addition, a second set of peaks at higher binding energy is visible for every element, comparable to the binding energies in Bi_2O_3, Sb_2O_3 and TeO_2. Since only one O 1s peak at 530.3 eV was observed, the film surface is most likely covered with a thin $Bi_{0.5}Sb_{0.5}Te_{3-x}O_x$ layer, which is expected since the film was handled and transferred under ambient conditions, leading to post-oxidation (surface oxidation) of the material. This was proven by an elemental depth profile analysis, showing a strong decrease of the oxidized species after a short sputtering period. After a sputtering time of 3 min, with an acceleration voltage of 3kV corresponding to an abrasion of about 10 nm equivalent to 10 quintuple layers, the intensity of peaks related to oxygen or carbon are below the detection limit.[64] The depth profile shows a nearly constant elemental composition along the growth direction in the bulk, whereas the surface is slightly tellurium rich. This is in good agreement with our previous reported measurements by scanning Auger electron microscopy (SAES) indicating a thin Te coverage of the surface caused by the enhanced retention time of the less volatile tellurium precursor compared to the antimony precursor inside the reactor.[52]

A TEM lamella was prepared by FIB technique to inspect the film-substrate system in cross section. Unfortunately, the sample shifted during the milling process, so the minimal thickness of the lamella could not be reached.

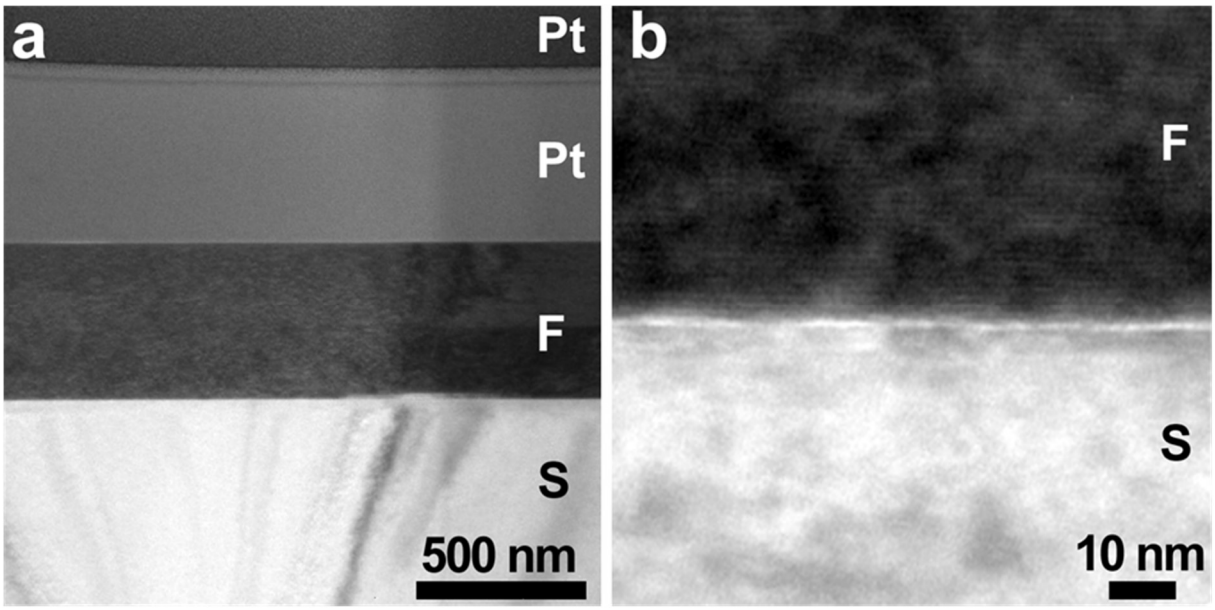

Fig. 7. Cross sectional TEM bright field images of a $(Bi_{0.5}Sb_{0.5})_2Te_3$ film grown at 400 °C on $Al_2O_3(0001)$ substrate (S: substrate, F: film, Pt: platinum layer).

However, TEM investigations show the $(Bi_{0.5}Sb_{0.5})_2Te_3$ film with an uniform thickness of 450 nm and a flat surface on the $Al_2O_3(0001)$ substrate (Fig. 7a). In addition, both platinum layers, which were deposited during the FIB process in order to protect the film, are visible, thereby the completeness of the film is ensured. An image at higher magnification (Fig. 7b) reveals a sharp interface between film and substrate showing a Fresnel contrast; an interfacial phase was not observed. Despite the unfavorable thickness of the sample, lattice fringes with a spacing of 1 nm parallel to the interface are imaged in the film. The spacing agrees to *d* value of the {0003} lattice planes of $(Bi_{0.5}Sb_{0.5})_2Te_3$. The lattice misfit for Al_2O_3 and $(Bi_{0.5}Sb_{0.5})_2Te_3$ is 5.6% for the d-spacings $\{\bar{1}2\bar{1}0\}$ and 9,3% for corresponding d-spacings along the *c**-axis {0006} in Al_2O_3 and {00015} in $(Bi_{0.5}Sb_{0.5})_2Te_3$, respectively. Misfit dislocations are not visible in this sample, maybe such contrasts are subdued by the thickness of the sample, but the bending contours in the substrate indicate some strain generated at the interface.

The selected area electron diffraction SAED pattern is shown in figure 8 for the substrate (a), the interface area(b) and the film (c along the $[10\bar{1}0]$ axis of Al_2O_3 and $(Bi_{0.5}Sb_{0.5})_2Te_3$, respectively. The diffraction patterns are rotated equivalent the orientation of the interface in Fig. 7. The 000*l* type reflections of the film and the substrate are in parallel direction, thus, the close packed layers of Al_2O_3 and $(Bi_{0.5}Sb_{0.5})_2Te_3$ propagate across the interface as was found by XRD results.

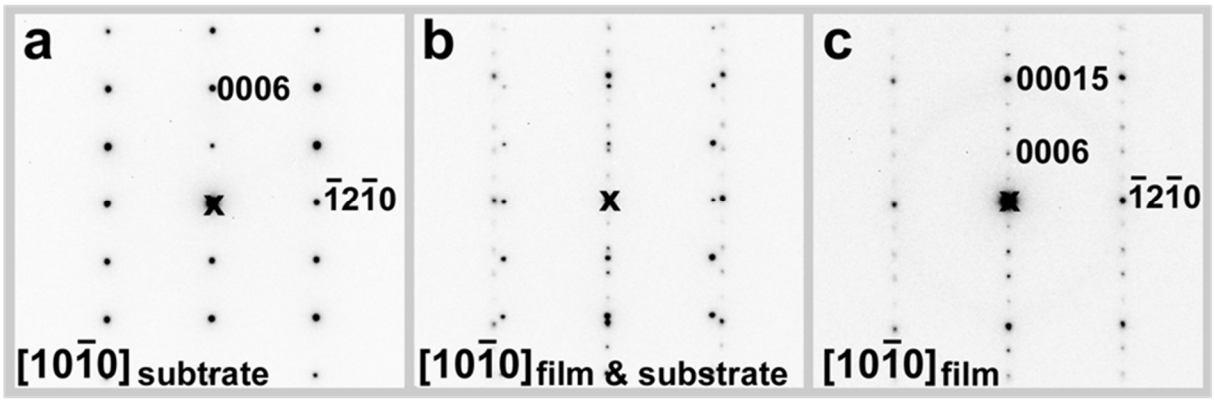

Fig. 8. SAED pattern of the $Al_2O_3(0001)$ substrate (a), the interface area (b) and the $(Bi_{0.5}Sb_{0.5})_2Te_3$ film (c) grown at 400 °C on $Al_2O_3(0001)$. The diffraction patterns are given with inverted contrast.

The in-plane orientation shows a perfect “hexagon on hexagon” orientation relationship. The $\{\bar{1}2\bar{1}0\}$ lattice planes of substrate and film coincidence with a small mismatch in the

<10$\bar{1}$0> direction as well as the {01$\bar{1}$0} lattice planes of the film and substrate were observed to match in the <2$\bar{1}\bar{1}$0> zone axis. The d-spacings of the film are bigger compared to the substrate which agrees to the smaller lattice parameters of the film.

The in plane transport properties of the MOCVD grown $(Bi_xSb_{1-x})_2Te_3$ films were determined by Hall effect measurements using the van der Pauw geometry in order to determine, how the carrier concentration *n*, the carrier mobility μ and the conductivity σ are affected by the bismuth content. For pure Sb_2Te_3 films, a high carrier mobility of about 330 $cm^2V^{-1}s^{-1}$ was found, comparable to values measured for bulk single crystals [65] as well as other high quality Sb_2Te_3 films grown by ALD, MOCVD and MBE.[45,66,67] It is noteworthy, that the carrier mobility in layered antimony or bismuth telluride films is greatly enhanced compared to polycrystalline films pointing to a preferred transport along the ab-plane, perpendicular to the c-axis. As shown in Fig. 9, with increasing bismuth content *x*, the carrier mobility decreases to a minimum value of 244 $cm^2V^{-1}s^{-1}$ for x = 0.63. With further increasing bismuth content, the mobility increases up to 260 $cm^2V^{-1}s^{-1}$ for pure Bi_2Te_3. Comparable results were observed by L.-P. Hu et al. for hot pressed bulk $(Bi_xSb_{1-x})_2Te_3$.[68]. A similar behavior of the carrier mobility for samples with high bismuth concentrations was reported by A. Kadhim et al. for bulk $(Bi_xSb_{1-x})_2Te_3$ samples obtained by solid-state microwave route.[69] They explained this effect by the decreased concentration of lattice defects, which leads to a subdued influence of the “alloy scattering” resulting in increasing carrier mobility. Zhang et al. reported on comparably high values for the carrier mobility for highly textured Sb_2Te_3 films with a maximum value of 305 $cm^2V^{-1}s^{-1}$ for 121 nm thick films grown by MBE on Si(111).[66]. For ALD fabricated films, Nielsch et al. found a similar value of about 270 $cm^2V^{-1}s^{-1}$.[67]. These findings are significantly higher compared to polycrystalline samples, for which Giani et al. in their pioneering work reported the best value of 196 $cm^2V^{-1}s^{-1}$. [70]

The pure Sb_2Te_3 film shows a high *p*-type carrier concentration of $p = 9.0\cdot10^{19}$ cm^{-3}. With increasing *x*, *p* drops to the minimum value of $1.5\cdot10^{19}$ cm^{-3} for x = 0.63. For Bi-richer films, *p* increases slightly to the maximum value of $3.0\cdot10^{19}$ cm^{-3} for pure Bi_2Te_3. The origin of the holes is the formation of antisite defects, i.e. the occupation of Te sites by Sb or Bi atoms in the tetradymite lattice, acting as acceptors. This can be expressed by the following equation, which is also valid for Bi_2Te_3:[71]

$$Sb_2Te_3 \leftrightarrow 2\,Sb_{Te}^{\bullet} + V_{Te}^{\bullet\bullet} + 2V_{Sb}''' + 3/2\,Te_2(g) + 2h^{\bullet}$$

For Bi_2Te_3, a second equation for the occupation of Bi sites by Te atoms leading to n-type material, can be formulated. The formation energy of antisite defects increases with increasing bond polarity. Based on the electronegativity χ (Pauling) for Bi(1.9), Sb(2.05) and Te(2.10), the formation energy for antisite defects is 0.35 eV for Sb_2Te_3 and 0.5 eV for Bi_2Te_3. Whereas Sb_2Te_3 is always p-type, Bi_2Te_3 can be p-type with excess Te and n-type with excess Bi.

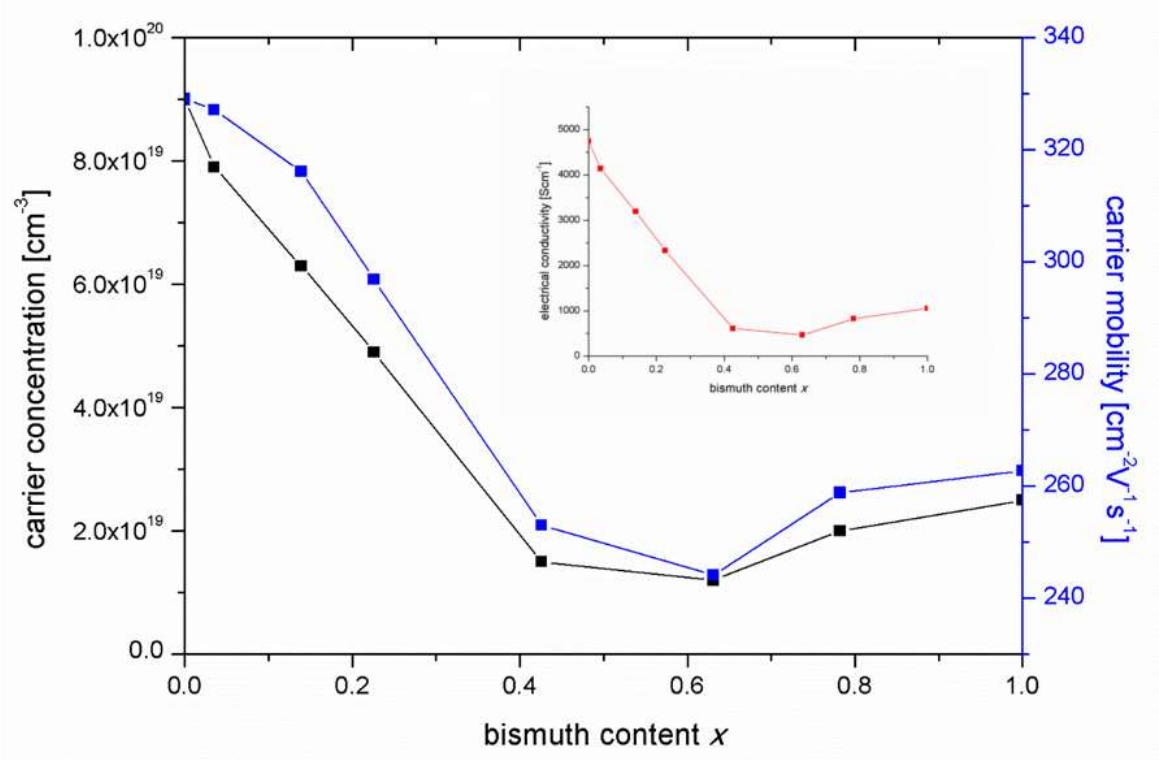

Fig. 9. Carrier concentration and mobility of $(Bi_xSb_{1-x})_2Te_3$ films grown at 400 °C on $Al_2O_3(0001)$.

Conclusion

We successfully grew epitaxial $(Bi_xSb_{1-x})_2Te_3$ films on commercially available, inexpensive $Al_2O_3(0001)$ substrates by MOCVD process using *tailor-made* metal organic precursors. The as-grown $(Bi_xSb_{1-x})_2Te_3$ films are crystalline and show a very smooth surface morphology as was proven by XRD, SEM, AFM and TEM. The transport properties strongly depend on the film composition and the carrier concentration can be tuned in a wide range. This is of particular interest for the thermoelectric properties of the films, since the Seebeck coefficient as well as the electrical and thermal conductivity strongly depends on the carrier concentration.

Acknowledgments

Stephan Schulz gratefully acknowledges financial support of the Deutsche Forschungsgemeinschaft (DFG) via the Priority Program SPP 1666 "*Topological Insulators*" and the University of Duisburg-Essen.

References

[1] Poudel B, Hao Q, Ma Y, Lan Y, Minnich A, Yu B, Yan X, Wang D, Muto A, Vashaee D, Chen X, Liu J, Dresselhaus M S, Chen G, Ren Z 2008 Science 320 634

[2] Xiao F, Hangarter C, Yoo B, Rheem Y, Lee K H, Myungj N V 2008 Electrochim. Acta 53 8103

[3] Beloborodov I S, Lopatin A V, Vinokur V M 2007 Rev. Mod. Phys. 79 469

[4] Snyder G J, Toberer E S 2008 Nat. Mater 7 105; Bell E L 2008 Science 321 1457

[5] Chen G, Dresselhaus M S, Dresselhaus G, Fleurial J P, Caillat T 2003 Int. Mater. Rev. 48 45

[6] Sommerlatte J, Nielsch K, Böttner H 2007 Phys. J. 6 35

[7] Xie W J, He J, Jung Kang H, Tang X F, Zhu S, Laver M, Wang, Copley J R D, Brown C M, Zhang Q, Tritt T M 2010 Nano Lett. 10 3283–89

[8] Zhao L D, Zhang B P, Li J F, Zhang H L, Liu W S 2008 Solid State Sci. 10 651–8

[9] Qi X L, Zhang S C 2010 Phys. Today 63, 33–8

[10] Bernevig B A, Hughes T L, Zhang S C 2006 Science 314 1757

[11] Hasan M Z, Kane C L 2010 Colloquium: Topological insulators. Rev. Mod. Phys. 82 3045

[12] Hsieh D, Xia Y, Qian D, Wray L, Dil J H, Meier F, Osterwalder J, Patthey L, Checkelsky J G, Ong N P, Fedorov A V, Lin H, Bansil A, Grauer D, Hor Y S, Cava R J, Hasan M Z 2009 Nature 460, 1101

[13] Zhang H, Liu C X, Qi X L, Dai X, Fang Z, Zhang S C 2009 Nat. Phys. 5 438

[14] Chen Y L, Analytis J G, Chu J H, Liu Z K, Mo S K, Qi X L, Zhang H J, Lu D H, Dai X, Fang Z, Zhang S C, Fisher I R, Hussain Z, Shen Z X 2009 Science 325 178

[15] Xia Y, Qian D, Hsieh D, Wray L, Pal A, Lin H, Bansil A, Grauer D, Hor Y S, Cava R J, Hasan M Z 2009 Nat. Phys. 5 398

[16] Koumoulis D, Leung B, Chasapis T C, Taylor R, King Jr. D, Kanatzidis M G, Bouchard L S 2014 Adv. Funct. Mater. 24 1519

[17] Niu C, Dai Y, Zhu Y, Ma Y, Yu L, Han S, Huang B 2012 Sci. Rep. 2 976

[18] Zhang G Q, Yu Q X, Wang W, Li X G 2010 Adv. Mater. 22 1959

[19] Heremans J P, Jovovic V, Toberer E S, Saramat A, Kurosaki K, Charoenphakdee A, Yamanaka S, Snyder G J 2008 Science 321 554

[20] Heremans J P, Thrush C M, Morelli D T 2004 Phys. Rev. B 70 115334

[21] Minnich A J, Dresselhaus M S, Ren Z, Chen G 2009 Energy Environ. Sci. 466

[22] Vineis C J, Shakouri A, Majumdar A, Kanatzidis M G 2010 Adv. Mater. 22 3970

[23] Lan Y C, Minnich A J, Chen G , Ren Z F 2010 Adv. Funct. Mater. 20 357

[24] Caillat T, Carle M, Pierrat P, Scherrer H, Scherrer S 1992 J. Phys. Chem. Solids 53 1121

[25] Caillat T, Gailliard L, Scherrer H, Scherrer S 1993, J. Phys. Chem. Solids 54 575

[26] Kim M Y, Yeo Y H, Park D H, Oh T S 2012 Ceram. Internat. 38S S529

[27] Xie W, Tang X, Yan Y, Zhang Q, Tritt T. 2009 M. J. Appl. Phys. 105 113713

[28] Fan X, Cai X, Rong Z, F Yang, Li G, Gan Z 2014 J. Alloys Comp. 607, 91

[29] Ma Y, Hao Q, Poudel B, Lan Y, Yu B, Wang D, Chen G, Ren Z 2008 Nano Lett. 82580

[30] Xie W, Tang X, Yan Y, Zhang Q, Tritt T M 2009 Appl. Phys. Lett. 94 102111

[31] Xie W, Wang S, Zhu S, He J, Tang X, Zhang Q, Tritt T M 2009 J. Mater. Sci. 48 2745

[32] Y. Xiao, J. Yang, G. Li, M. Liu, L. Fu, Y. Luo, W. Li, J. Peng, Intermetallics 2014, 50, 20

[33] Zhang Y, Stucky G D 2014 Chem. Mater. 26 837

[34] Zheng Z H, Fan P, Luo J T, Cai X M, Liang G X, Zhang D P, Ye F 2014 Thin Solid Films 562 181

[35] He X, Guan T, Wang X, Feng B, Cheng P, Chen L, Li Y, Wu K 2012 Appl. Phys. Lett. 101 123111

[36] Desai C F, Chourasia N C, Dhar S N 2000 Mater. Lett. 45 116

[37] Jimenez S, Perez J G, Tritt T M, Zhu S, Sosa-Sanchez L J, Martinez-Juarez J, López O 2014 Energy Conversion and Management 87 868

[38] Kim S S, Yamamoto S, Aizawa T 2004 J. Alloys Compd. 375 107

[39] Zhu W, Deng Y, Wang Y, Luo B, Cao L 2014 Thin Solid Film 556 270

[40] Li F, Wang W 2009 Appl. Surf. Sci. 255 4225.

[41] Rowe D M 1995 CRC Handbook of Thermoelectrics CRC Press, Boca Raton, FL

[42] Erdoğan I J, Demir U 2010 Electrochim. Acta. 55 6402

[43] Song J, Yao Q, Wu T, Shi X, Chen L 2013 Electron. Mater. Lett. 9 709

[44] Venkatasubramanian R, Colpitts T, Watko E, M. Lamvik, El-Masry N 1997 J. Cryst. Growth 170, 817

[45] Venkatasubramanian R, Siivola E, Colpitts T, O'Quinn B 2001 Nature, 413 597

[46] Aboulfarah B, Mzerd A, Giani A, Boulouz A, Delannoy F P, Foucaran A, Boyer A 2000 Mater. Chem. Phys. 62 179

[47] Wang G, Endicott L, Uher C 2011 Sci. Adv. Mater. 3 1

[48] Winkler M, Liu X, Schürmann U, König J D, Kienle L, Bensch W, Böttner H 2012 Z. Anorg. Allg. Chem. 2441

[49] Kim J H, Jeong D Y, Kim J S, Ju B K 2006 J. Appl. Phys. 100 123501

[50] Boulouz A, Giani A, Sorli B, Koutti L, Massaq A, Pascal-Delannoy F 2014 J. Mater. 430410

[51] He L, Kou X, Lang M, Choi E S, Jiang Y, Nie T, Jiang W, Fan Y, Wang Y, Xiu F, Wang K L 2013 Sci. Rep. 3 3406

[52] Bendt G, Zastrow S, Nielsch K, Mandal P S, Sánchez-Barriga J, Rader O, Schulz S 2014 J. Mater. Chem. A 2 8215

[53] Chen M T, George J W 1968 J. Organometal. Chem. 12 401

[54] M. Wieber 1981 Gmelin Handbook of Inorganic Chemistry, 8th ed., Sb Organoantimony Compounds Part 1, Ed. H. Bitterer, Springer Verlag Berlin.

[55] Gilman H, Nelson J F 1937 J. Am. Chem. Soc. 59 935

[56] Jones A C, O'Brien P, 1997 CVD of Compound Semiconductors: Precursor Synthesis, Development and Applications VCH 212

[57] Irvine S J C, Mullin J B, Giess J, Gough J S, ROYLE A 1988 J. Crystal Growth 1988 93 732

[58] Ewan A, McQueen D, Peter N. Cuishaw, John C. Walton, D.V. Shenai-Khatkhate, David J. Cole-Hamilton, Journal of Crystal Growth 107 (1991) 325—330

[58] McAllister T 1989 J. Crystal Growth 96 552

[60] McDaniel A H, Liu B, Hicks R F 1992 J. Crystal Growth 124 676

[61] Kuhn W S, Qu'Hen B, Gorochov O 1995 Prog. Crystal Growth and Charact. 31 1

[62] Kisker D W, Steigerwald M L, Kometani T Y Jeffers K S 1987 Appl. Phys. Letters 50 1681

[63] Krumraina J, Musslera G, Borisovaa S, Stoicaa T, Plucinskib L, Schneider C M, Grützmacher D 2011 j. Cryst. Growth 324 115

[64] Note that the abrasion of material by sputtering is calibrated on silicon; no data are available for $(Bi_xSb_{1-x})_2Te_3$ so the given value is a rough approximation.

[65] Scherrer H, Scherrer S 1995 D.M. Rowe (Ed.), CRC Handbook of Thermoelectrics, CRC Press New York 211

[66] Zhang X, Zeng Z, Shen C, Zhang Z, Zang Z, Lin C, Hu Z 2014. Appl. Phys. 115 024307

[67] Zastrow S, Gooth J, Boehnert T, Heiderich S, Toellner W, Heimann S, Schulz S, Nielsch K 2013 Semicond. Sci. Technol. 28 035010

[68] Hu L P, Zhu T J, Wang Y G, Xie H H, Xu Z J, Zhao X B 2014 NPG Asia Materials 6 1

[69] Kadhim A, Hmood A, Hassan H A 2012 Mater. Sci. Semicond. Process. 15 549

[70] B. Aboulfarah, A. Mzerd, A. Boulouz, A. Giani, A. Foucaran, A. Boyer, M. 1998 J. Condensed Matter. 1 100.

[71] Z. Stary, J. Horak, M. Stordeur, M. Stölzer 1988J. Phys. Chem. Solids 49 29.

Supporting information

Van der Waals epitaxial MOCVD-growth of $(Bi_xSb_{1-x})_2Te_3$ (0<x<1) films

G. Bendt,[1] J. Sonntag,[2] A. Lorke,[2] W. Assenmacher,[3] U. Hagemann,[4] S. Schulz[1]*

Content

Fig. S1: DSC Et_3Bi.

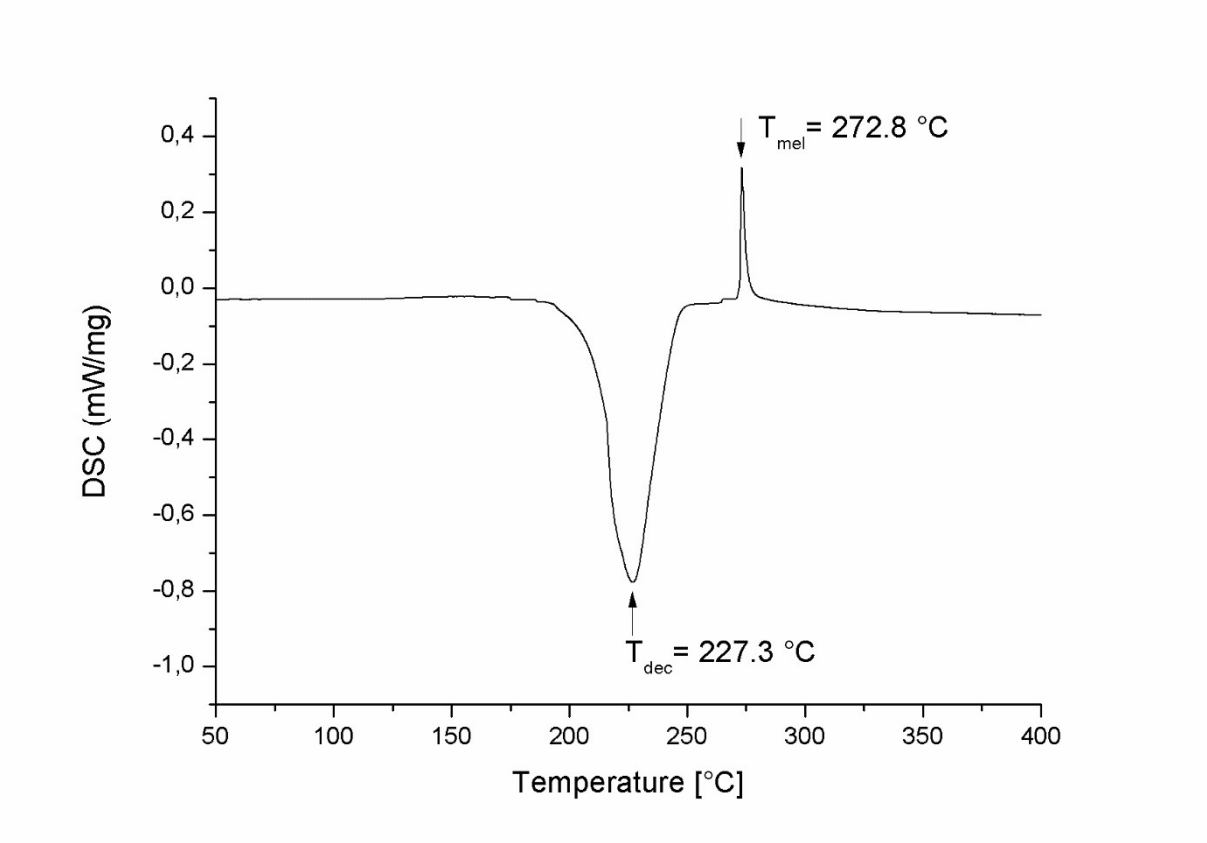

Fig S2: XPS elemental depth profile of the $(Bi_{0.2}Sb_{0.8})_2Te_3$ film grown on $Al_2O_3(0001)$ measured at two different positions of the film.

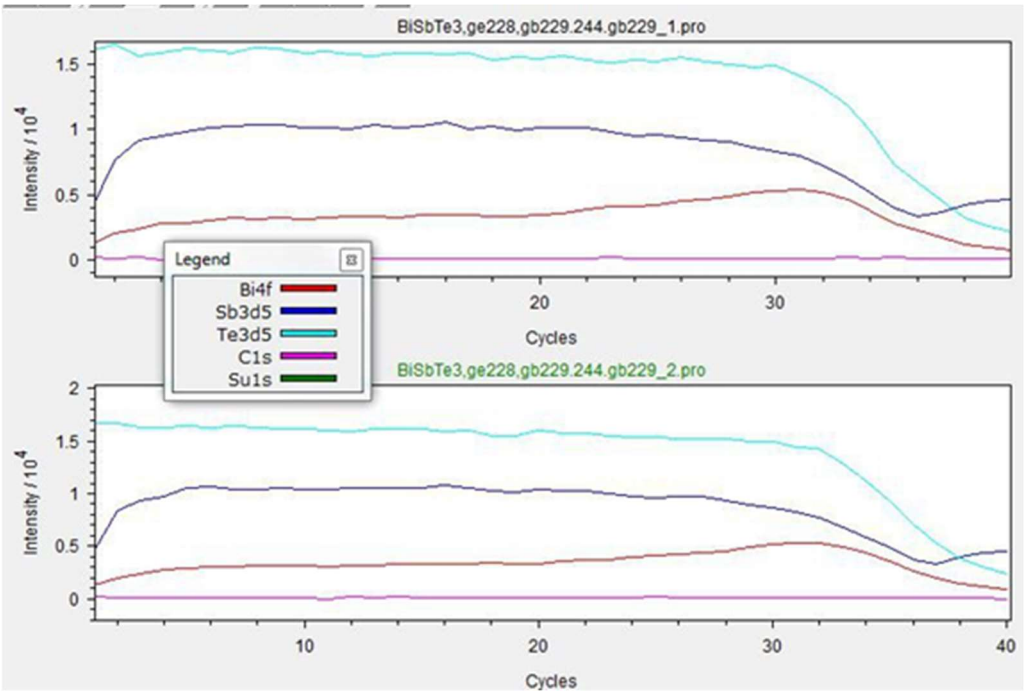

Fig S3: X-Ray photoelectron spectrum of the $(Bi_{0.5}Sb_{0.5})_2Te_3$ film grown on $Al_2O_3(0001)$.

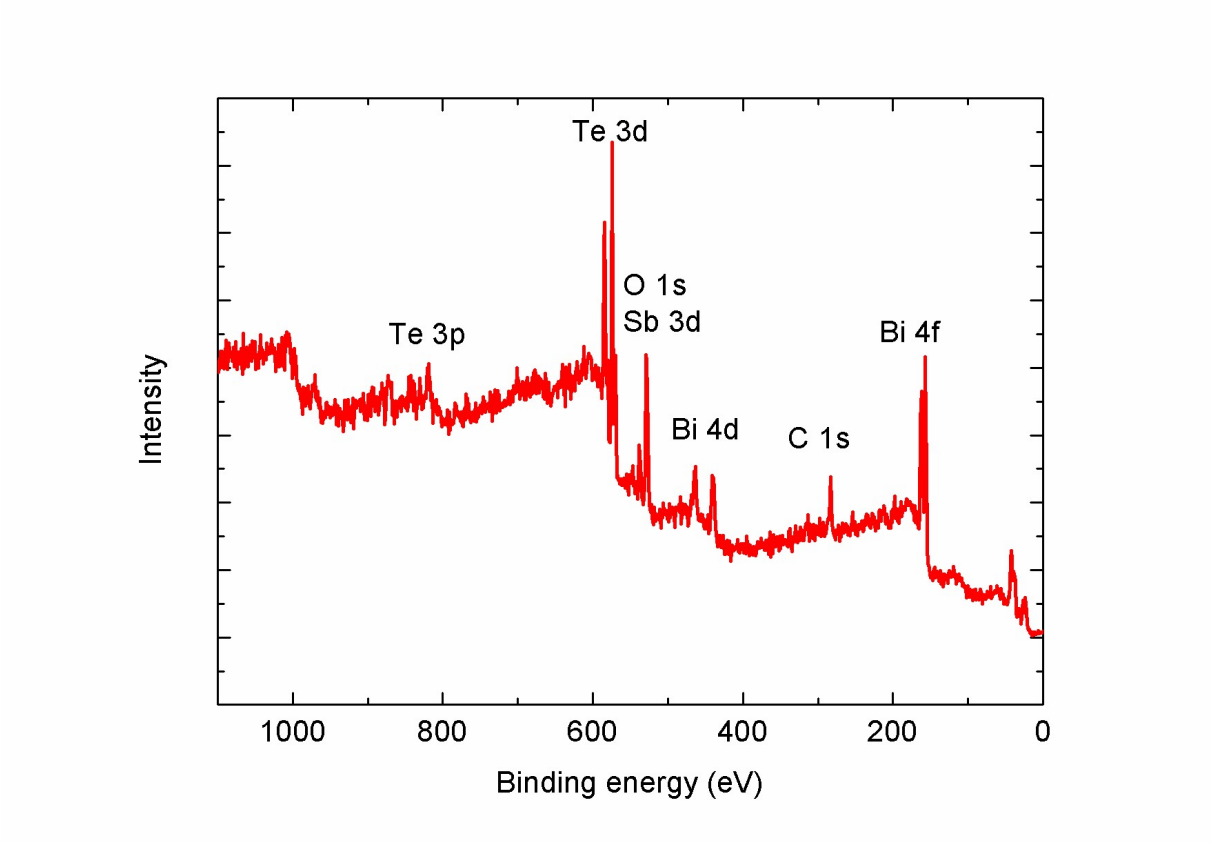

DOI: 10.1088/0268-1242/30/8/085021
URN: urn:nbn:de:hbz:464-20201125-115425-8

This is the **Accepted Manuscript** version of an article accepted for publication in *Semiconductor Science and Technology* 2015, 30, 085021. IOP Publishing Ltd is not responsible for any errors or omissions in this version of the manuscript or any version derived from it. The Version of Record is available online at https://doi.org/10.1088/0268-1242/30/8/085021